https://doi.org/10.1007/s41230-021-9012-6

Microstructure and corrosion resistance of Ti-Ni/steel composite materials

***Long You[1, 2], Chang-ji Wang[2, 3], Zhou Wang[1], Kun-ding Liu[1]**

1. School of Materials Science and Engineering, Henan University of Science and Technology, Luoyang 471003, Henan, China

2. Henan Key Laboratory of High-temperature Structural and Functional Materials, Henan University of Science and Technology, Luoyang 471003, Henan, China

3. National Joint Engineering Research Center for Abrasion Control and Molding of Metal Materials, Henan University of Science and Technology, Luoyang 471003, Henan, China

Abstract: Ti-Ni composite sub-micron powders with different compositions were prepared by vacuum melting and atomization technology. These powders, after being mixed with a solution of phenolic resin and alcohol, were applied on the mold cavity wall, by which a casting-infiltration layer was introduced on the surface of ZG45 steel via reactions between the powders and molten steel under the heat released by solidification. The effects of the powders' composition and pouring temperature on the corrosion resistance of the casting-infiltration layer were studied. An optimal casting-infiltration layer with a thickness of ~7 mm was obtained by infiltrating the Ti-Ni composite powders containing 35wt.% Ti to ZG45 steel pouring at 1,650 °C. The casting-infiltration layer has a good metallurgic bonding with the matrix, and is mainly composed of Fe_2Ti phase and continuous γ-(Fe, Ni) solid solution. In the corrosive H_2SO_4 solution, the corrosion potential of the casting-infiltration layer is lower than the matrix, tending to form a passivation film, which lowers the dissolution rate especially when the potential rises to 0.50 V. After dipping in the 10wt.% NaCl solution for 480 h, a lot of corrosion holes appear in the ZG45 steel matrix, while there are no obvious traces of corrosion on the casting-infiltration layer.

Key words: Ti-Ni composite; casting-infiltration layer; corrosion resistance

CLC numbers: TG146.23 **Document code:** A **Article ID:** 1672-6421(2021)05-505-08

1 Introduction

Steel materials are inevitably corroded by the atmosphere, impurities or liquids, when they are widely applied to machinery, oil pipelines and so on [1-4]. One study found that the fatigue life of steel wire was decreased by about 99% if there was a tiny corrosion pit with a size of 0.2–0.6 mm, accompanied by an extremely serious damage consequence [5]. Therefore, ways to improve the corrosion resistance of steel materials at the minimum cost has been of concern. An important way to improve corrosion resistance is to avoid chemical reactions between the steel materials and the medium, especially to prevent Fe from forming galvanic cells with other elements in the steel [6-10].

Some corrosion-resistant elements were added during melting to change the structure of the steel materials and improve corrosion resistance, such as martensitic stainless steel, ferritic stainless steel and austenitic stainless steel [11-14]. For example, adding a small amount of 0.05wt.% Sn greatly improved the corrosion resistance of steel, including the ability to resist point corrosion [15-18]. Local alloying or coating technology can prevent corrosion and oxidation under various harsh environments via a protective layer synthesized on the surface, without changing the composition, structure and properties of the matrix [19-21]. Zhang et al. [22] used the grid-enhanced plasma surface modification method to prepare the TiN coating on the surface of ZG45 steel. The experimental results showed that the TiN coating displayed excellent corrosion resistance. Uusitalo et al. [23] synthesized a Ni-57CrMoSiB coating on the surface of boiler steels using high velocity oxy-fuel spraying (HVOF), and suggested that the coating was covered by a protective oxide scale to protect the boiler steels from corrosion attack in high-temperature oxidizing conditions.

However, the non-matrix-melting surface technologies face great challenges in the bonding quality between the coating and the matrix. Casting

***Long You**

Male, born in 1983, Ph.D. His research interests mainly focus on microstructure and properties of wear resistant steels and their casting and solidification process simulation. To date, he has published about 20 papers.

E-mail: youlong25@163.com;

Received: 2020-12-28; Accepted: 2021-06-21

infiltration technology has thus been recommended among the most widely used technologies for preparing protective coatings on a metal matrix [24-26]. Corrosion-resistant materials or raw materials were coated or pressed onto the cavity wall of casting molds. As the molten metals were poured, under the heat released by solidification, a casting-infiltration layer showing a good bonding interface with the matrix was obtained [27]. Szymański et al. [28] successfully prepared a TiC-containing composite layer on Fe matrix after the liquid steel was poured at 1,823 K. Experimental tests proved that its comprehensive mechanical properties significantly increased compared with the matrix. Zhao et al. [29] used a combination method of casting and heat treatment to obtain a TaC coating, adjacent to a transition region containing Ta, TaC, and Fe_3C on the surface of the cast iron matrix.

Using the vacuum infiltration casting technology, Yang et al. [30] fabricated a Ni-based composite layer on ZQAl9-4 bronze. The composite layer was formed via metallurgical fusing caused by the solidification heat of the matrix. However, the transition layer between the Ni-based composite layer and the matrix (ZQAl9-4) was formed via diffusion and solution with the matrix, which was regarded as a key process of achieving the excellent metallurgical bonding of the interface.

In this study, the casting infiltration method was applied to synthesize a protective layer on ZG45 steel. Ti was chosen as the main element of the casting-infiltration powder due to the advantages of low density, high specific strength and outstanding resistance to pitting and acid corrosion [31-33]. However, high activity renders the metallic Ti unsuitable as the casting-infiltration raw material, hence Ti-Ni alloy powders were used to prepare the protective layer. Ni element is vital in forming a good metallurgical bonding interface with the steel matrix, since it can form continuous solid solution with Fe. The heat released by temperature decrease and solidification of molten ZG45 steel was utilized to melt the Ti-Ni composite powders, which reacted with the steel matrix and formed a corrosion-resistant casting-infiltration layer. The effects of Ti-Ni powders' composition and casting parameters on the structure and corrosion resistance of the casting-infiltration layer were studied.

2 Experimental procedure

ZG45 steel was selected as the matrix material. The Ti-Ni alloy powders were used as casting-infiltration materials, and their composition range was designed in the low melting point zone according to Fe-Ni-Ti ternary phase diagram in Fig. 1. The Ti-Ni alloy powders were obtained via atomization method, and consist of 35wt.%, 55wt.% and 75wt.% Ti, respectively. The CO_2-cured water glass sand moulds with the dimensions of 100 mm×80 mm×50 mm were used. The phenolic resin (60wt.%) and alcohol (40wt.%) were mixed to prepare a solution. Subsequently, the Ti-Ni alloy powders were mixed with the obtained solution in a ratio of 3:1 by weight, and then coated on the mold cavity wall using a manual method, followed by curing and drying. The thickness of the coating was 8–10 mm. The ZG45 steel was melted in a medium-frequency induction furnace and then poured into the mold cavity at 1,550–1,650 °C. The powder in the coating was melted by the heat of molten metal at high temperature, and after reactions and solidification, the cast-infiltration layer covering the steel materials was obtained.

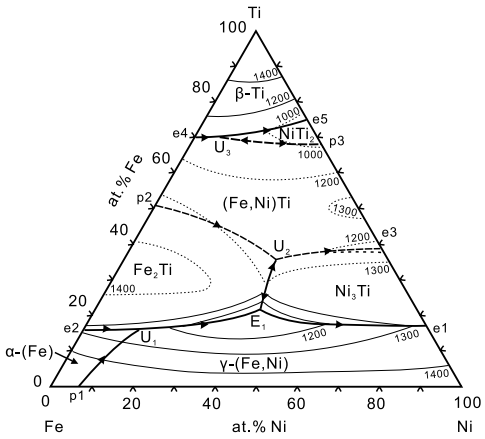

Fig. 1: Fe-Ni-Ti phase diagram [34]

The samples for corrosion tests were cuboid with a length of 10 mm, a width of 10 mm and a thickness of 20 mm. An electrochemical workstation (CHI660D) was employed to test the corrosion resistance of the cast-infiltration layer. These corrosion experiments were performed in 3.5wt.% NaCl solution and 1 mol·L^{-1} H_2SO_4 solution, respectively, by using a three-electrode system, with the cast-infiltration layer of the sample as the working electrode, graphite electrode as the auxiliary electrode and saturated calomel electrode as the reference electrode. The working electrode area of the cast-infiltration layer was 1 cm^2. Three sets of tests were performed on each of these samples under the same condition. In addition, the static corrosion tests were carried out to investigate the corrosion resistance of the cast-infiltration layer by simulating seawater environment in the 10wt.% NaCl solution. The corrosion period was set as 120, 240, 360 and 480 h, and the corrosion performance of the cast-infiltration layer was evaluated by referring to the weight loss after corrosion. The morphology, microstructure and constitution of the casting-infiltration layer and the matrix were observed and analyzed by means of SEM-EDAX, TEM and XRD.

3 Results and discussion

3.1 Thermodynamic analysis of casting-infiltration layer

According to the phase diagram of Fe-Ni-Ti system in Fig. 1, the following reactions may occur:

$$Fe + Ti = TiFe \quad (1)$$

$$2Fe + Ti = TiFe_2 \quad (2)$$

$$Ti + Ni = TiNi \quad (3)$$

$$2Ti + Ni = Ti_2Ni \quad (4)$$

$$Ti + 3Ni = TiNi_3 \quad (5)$$

The relationship between reaction enthalpy ΔG_T^{Θ} and temperature can be expressed by the Gibbs-Helmholtz equation:

$$d\left(\frac{\Delta G_T^{\Theta}}{T}\right) = -\frac{\Delta H_T^{\Theta}}{T^2}dT \quad (6)$$

where ΔH_T^{Θ} is the standard molar enthalpy of reaction, and T is the thermodynamic temperature, which can be obtained by Kirchhoff's formula:

$$d\Delta H_T^{\Theta} = \Delta C_p dT \quad (7)$$

$$\Delta C_p = \Delta a + \Delta bT + \Delta cT^{-2} \quad (8)$$

where, ΔC_p is the difference between standard molar specific heat of product and reactant at a constant pressure, Δa, Δb, Δc are the differences in coefficients at different temperatures.

Equation (8) is substituted into Eq. (7), getting the following equation after integrals:

$$\Delta H_T^{\Theta} = \Delta H_0 + \Delta aT + \frac{1}{2}\Delta bT^2 - \Delta cT^{-1} \quad (9)$$

where ΔH_0 is the standard molar enthalpy of formation.

Equation (9) is substituted into Eq. (6), getting the following equation after integrals:

$$\Delta G_T^{\Theta} = \Delta H_0 - \Delta aT\ln T - \frac{1}{2}\Delta bT^2 - \frac{1}{2}\Delta cT^{-1} + YT \quad (10)$$

where Y can be obtained based on the values of ΔH and ΔG_{298}^{Θ} at $T = 298$ K.

$$Y = (\Delta G_{298}^{\Theta} - \Delta H_0)(298)^{-1} + \Delta aT\ln T + \frac{1}{2}\Delta b(298) + \frac{1}{2}\Delta c(298)^{-2} \quad (11)$$

After the Y values are calculated, the change in the Gibbs free energy in Eqs. (1) to (5) can be calculated according to Eq. (10), as shown in Fig. 2. Within the temperature range of 400–1,800 K, the change of the standard Gibbs free energy of each reaction is less than zero, indicating that these reactions can occur spontaneously under these conditions. Generally, the stability of the products increases with the increase of the absolute value of Gibbs free energy change, so intermetallics $TiNi_3$ and $TiFe_2$ are the most stable phases in the Fe-Ni-Ti system. However, according to the Fe-Ni binary phase diagram [35], Fe and Ni continue to solubilize each other in a large range of temperatures. This suggests that Fe and Ni may first form the solid solution rather than $TiNi_3$, TiNi and Ti_2Ni.

3.2 Microstructure and characterization of casting-infiltration layer

Figure 3 shows the SEM images, corresponding EDS, and XRD patterns of Ti-Ni composite powders with different Ti contents prepared by the atomization method. Observation and

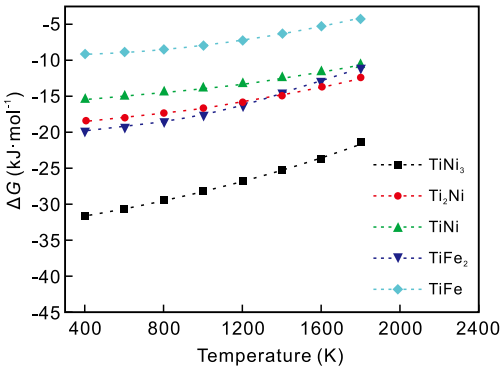

Fig. 2: Changes of Gibbs free energy of Fe-Ni-Ti alloys at different temperatures

analysis using SEM-EDAX show the prepared powders exist as even spherical particles in the size range of 50–150 μm, as shown in Fig. 3(a–c). This powder size was confirmed to be more suitable for forming casting-infiltration layer [36], which can avoid the phenomena of the excessive fine particles being washed away from the mold cavity and the coarse particles being retained as unmelted inclusions. As can be seen from Fig. 3(d), the Ni-35wt.% Ti alloy powder is mainly composed of NiTi and Ni_4Ti_3, with a small amount of metallic Ni. The Ni-55wt.% Ti alloy powder mainly consists of Ni_2Ti. With the Ti addition increasing to 75wt.%, there is a small amount of metallic Ti in the Ti-Ni alloy powder in addition to Ni_2Ti.

The pouring temperature of the molten steel has a direct influence on the formation of the casting-infiltration layer. Based on the phase diagram of the Fe-Ni-Ti system (Fig. 1) and previous experiences, the pouring temperature was set in the range of 1,500–1,700 °C. Figures 4(a) and (b) show the surface morphology and cross-section images of the casting-infiltration layer prepared at 1,550 °C and 1,650 °C using the Ni-35wt.% Ti powders. It can be seen that a large number of holes exist on the surface of the casting-infiltration layer when the pouring temperature was 1,550 °C, and the thickness of the layer is about 7 mm. Actually, most of the released solidification heat is consumed rapidly through the cavity wall during the casting process. So, the residual solidification heat for completely melting the Ti-Ni alloy powder is insufficient when the pouring temperature is relatively low, then, a lot of holes and slags appear in the casting-infiltration layer. As the pouring temperature increases to 1,650 °C, a high-quality casting-infiltration layer with thickness of ~7 mm is obtained on the surface of ZG45 steel matrix, with no holes and slags, as shown in Fig. 4(b), and a smooth interface between the casting-infiltration layer and the matrix was obtained.

The composition of raw materials is also one of the important factors for obtaining an ideal casting-infiltration layer. Figures 4[(b)–(d)] show the macroscopic morphological images of casting-infiltration layers with different Ti addition at the pouring temperature of 1,650 °C. With the Ti content increasing to 55wt.% and 75wt.%, more and more pores and pits are observed in the casting-infiltration layer. This is mainly because the chemical reactions are completed in a very short time to avoid Ti oxidation when Ti content is as low as 35wt.%.

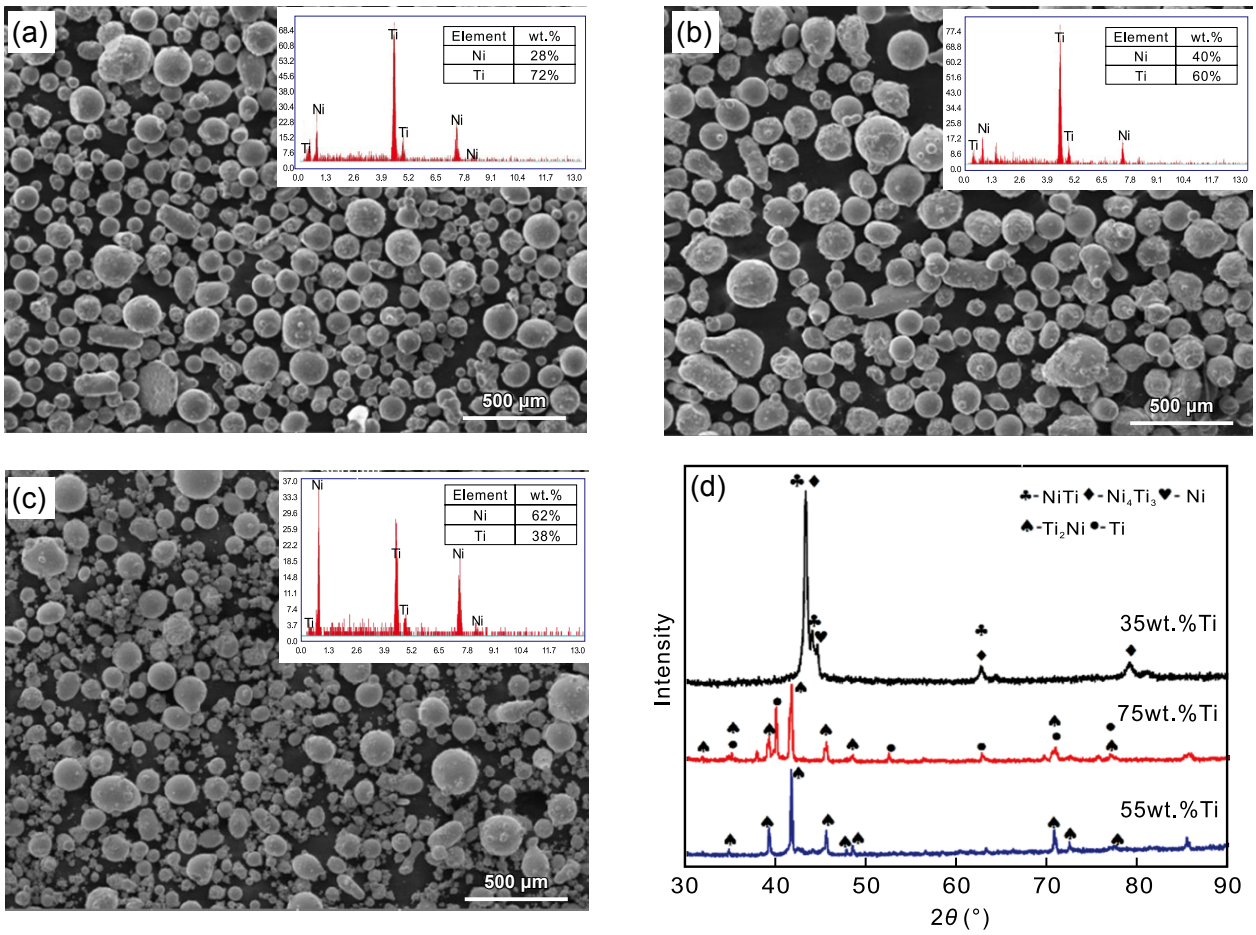

Fig. 3: SEM image and corresponding EDS of Ni-75wt.%Ti (a), Ni-55wt.%Ti (b), and Ni-35wt.%Ti alloy powders (c), and their XRD patterns (d)

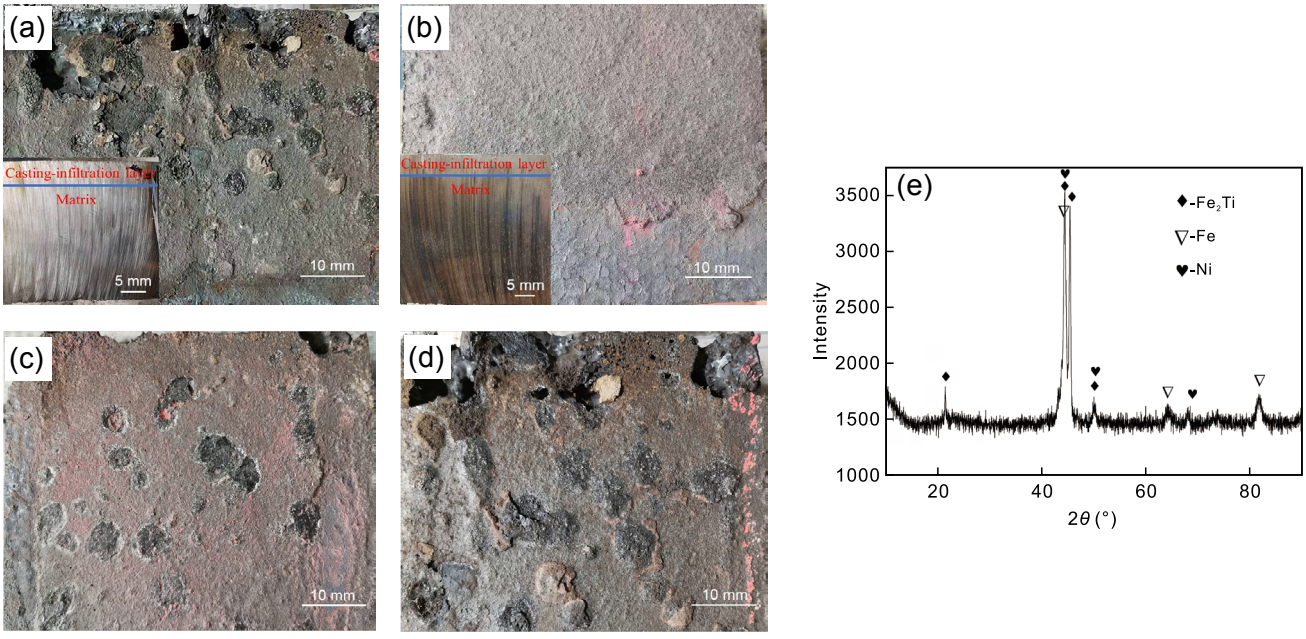

Fig. 4: Surface morphology and cross-section images (at the lower left of the figure) of casting-infiltration layer with Ni-35wt.% Ti powder prepared at 1,550 °C (a) and 1,650 °C (b); surface morphology of the layer with Ni-55wt.% Ti (c) and Ni-75wt.% Ti (d) prepared at 1,650 °C; and XRD pattern of casting-infiltration layer prepared using Ni-35wt.%Ti powder at 1,650 °C (e)

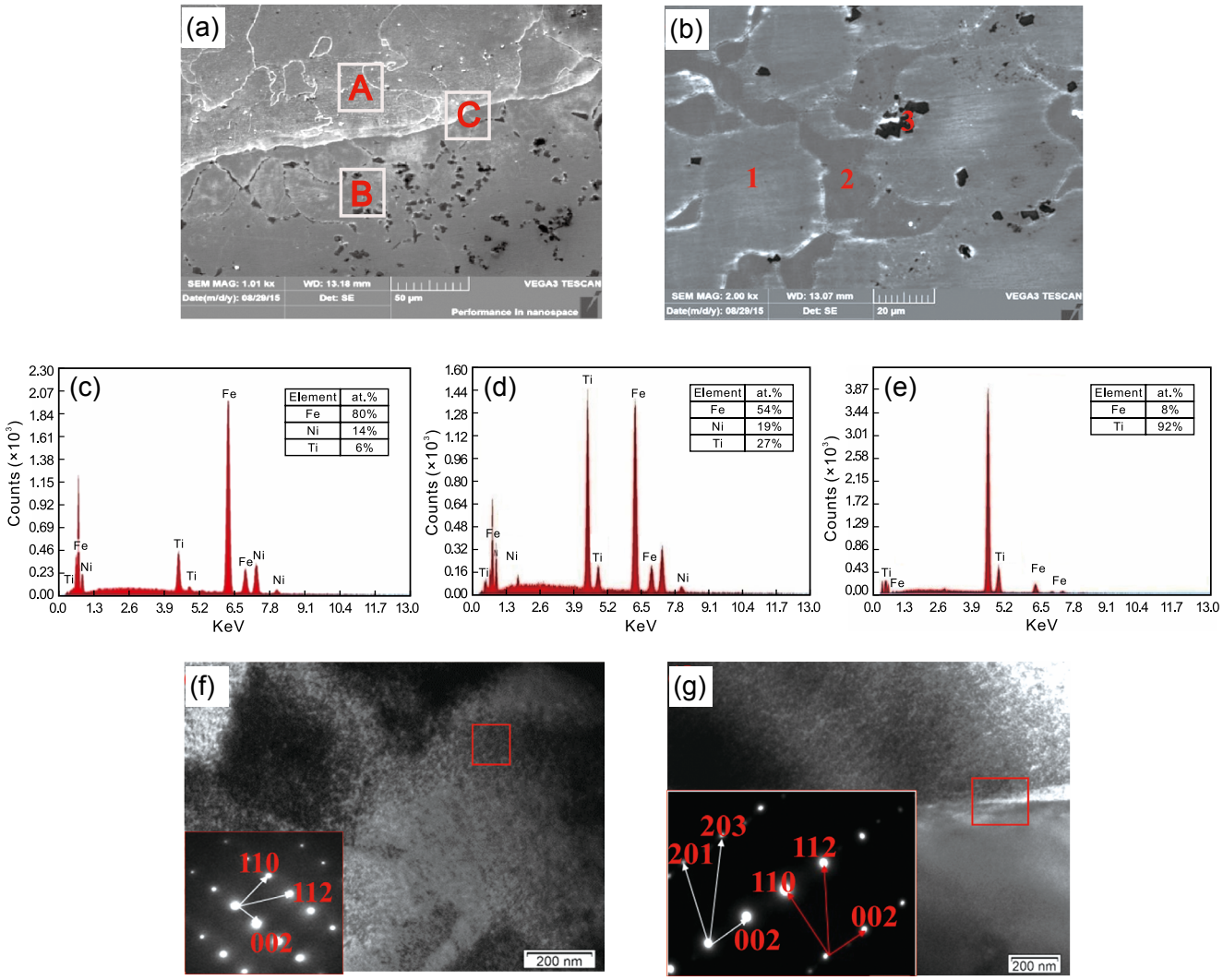

Fig. 5: SEM image of composite material with Ni-35wt.% Ti prepared at 1,650 °C (a), Areas A, B, C represent matrix, casting-infiltration layer and the interface, respectively; SEM image of Area B (b), with EDAX patterns of Spots 1, 2, 3 shown in (c–e), respectively; (f–g) HRTEM image of Areas A and C with diffraction pattern of the red box area, respectively

However, with Ti content increasing up to 55wt.% and 75wt.%, the oxidation of Ti atoms inevitably occurs, and the surface oxides easily peel off, as shown in Figs. 4(c) and (d).

The alloy powder and steel matrix diffuse to each other which is confirmed by the emergence of Fe_2Ti in the casting-infiltration layer [Fig. 4(f)]. The casting-infiltration layer and the matrix were further characterized by means of SEM-EDAX and HRTEM, as shown in Fig. 5. Combined with XRD and EDAX analysis, the casting-infiltration layer is composed of Fe_2Ti, Ti and γ-(Fe, Ni). HRTEM images and diffraction patterns in Figs. 5(f) and (g) show that the solid solution γ-(Fe, Ni) is formed in the matrix, and the mixture of Fe_2Ti and γ-(Fe, Ni) is formed at the interface between the matrix and the infiltration layer. The casting-infiltration layer forms a good metallurgic bonding with the matrix, and no defects and inclusions are found along this interface, as shown in Fig. 5(a).

The Ni-35wt.% Ti alloy powder mainly consists of NiTi and Ni_4Ti_3 and a small amount of metallic Ni. Combined with thermodynamic analysis, it is believed that these intermetallic compounds are decomposed into Ni and Ti during the casting process. Ni dissolves into Fe to form a solid solution γ-(Fe, Ni) in the matrix, as indicated by the diffraction pattern in Fig. 5(f), while the residual Fe reacts with Ti to form the most stable Fe_2Ti, as indicated by the diffraction pattern in Fig. 5(g). Therefore, the casting-infiltration layer is mainly composed of Fe_2Ti, γ-(Fe, Ni) and a small amount of metallic Ti gathering around Fe_2Ti.

3.3 Enhanced corrosion behavior of casting-infiltration layer

Figure 6(a) shows the polarization curves of the casting-infiltration layer and ZG45 matrix in 1 mol·L^{-1} H_2SO_4 solution. With the increase of potential at the beginning, the current density of the casting-infiltration layer and matrix decreases gradually. The current density of casting-infiltration layer is lower than the matrix, indicating that the dissolution rate of the casting-infiltration layer is faster than that of the matrix. However, when the potential increases to the self-etching potential −0.40 V of the casting-infiltration layer, the anodic polarization occurs, and both current density and dissolution

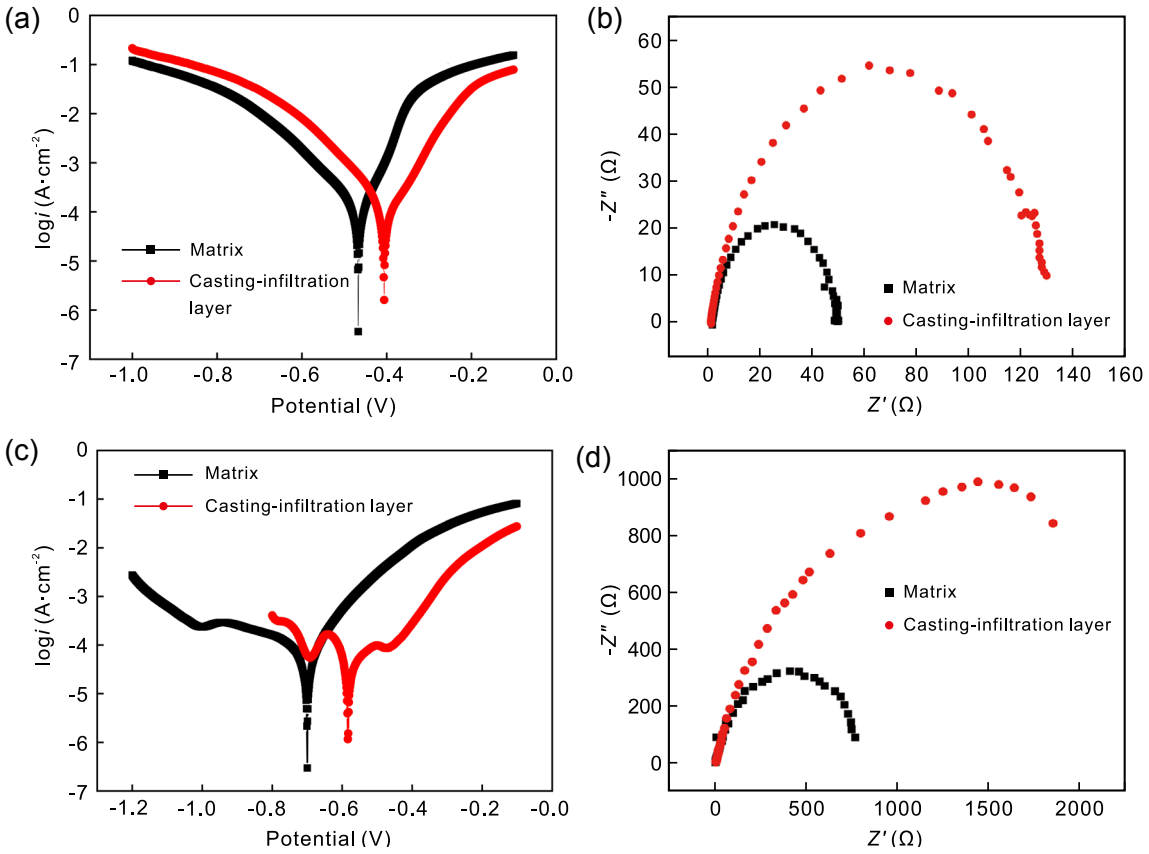

Fig. 6: Polarization (a, c) and AC impedance (b, d) curves of Ni-35wt.%Ti layer and ZG45 steel matrix in 1 mol·L^{-1} H_2SO_4 solution (a, b) 3.5wt.% NaCl solution (c, d)

rate of the casting-infiltration layer are lower than that of the matrix. With the potential further raises to –0.49 V, the matrix suffers from anodic polarization, and then the dissolution rate increases. Generally, the higher self-corrosion potential represents the outstanding corrosion resistance [37]. With a higher self-corrosion potential, the casting-infiltration layer possesses an enhanced resistance to corrosion compared with the matrix. Figure 6(b) shows the comparison of AC impedance curves between the casting-infiltration layer and matrix in 1 mol·L^{-1} H_2SO_4 solution. The curves of the casting-infiltration layer and matrix are similar, and both of them consist of high frequency induced reactance arc, capacitive reactance arc and low frequency small capacitive reactance arc. The radius of the high frequency capacitive reactance arc is positive correlation with the corrosion resistance of compounds during electrochemical reactions, so the casting-infiltration layer with a larger radius of capacitance reactance arc has a higher corrosion resistance.

In the 3.5wt.% NaCl solution, the polarization curve of the matrix is similar to that in 1 mol·L^{-1} H_2SO_4 solution, but the polarization curve of the casting-infiltration layer varies greatly, as shown in Fig. 6(c). When the potential increases to the self-corrosion potential of -0.58 V of the casting-infiltration layer, the anodic polarization occurs, and then the electrochemical reactions convert into a passivation state with the potential further rising to -0.50 V.

In contrast to the ZG45 steel matrix, an increment of 120 mV in the self-corrosion potential also indicates that the casting-infiltration layer has a higher resistance to corrosion attack. By comparing the AC impedance curves in 3.5wt.% NaCl solution in Fig. 6(d), the casting-infiltration layer with a larger radius of capacitance-reactance arc is also ascertained to have an improved corrosion resistance compared to the matrix.

Additionally, static corrosion tests were carried out to investigate the corrosion resistance of the casting-infiltration layer by simulating a seawater environment in 10wt.% NaCl solution. According to the weight changes in samples before and after corrosion, the weight loss per unit area was calculated, and the variation curve of the corrosion rates is plotted in Fig. 7(a). With the extension of dipping time, the corrosion velocity of the casting-infiltration layer decreases at first and then increases gradually. A passivation film should be formed on the surface of the casting-infiltration layer in the starting stage, which slows down the corrosion process at lower rates. However, with the extending of immersion time, part of surface passivation film dissolves and the corrosion rate slightly increases. Comparatively, the corrosion rate of the matrix rapidly increases with the increasing immersion time, showing that there is no passivation film formed on the surface of the matrix. Figures 7(b) and (c) show the morphology of the eroded samples after dipping for 480 h. The surface of ZG45 steel matrix is filled with erosion holes, and some of them expand and connect with each other to form deep gullies, causing serious damage to the matrix [Fig. 7(b)]. Nonetheless, there are no obvious traces of corrosion

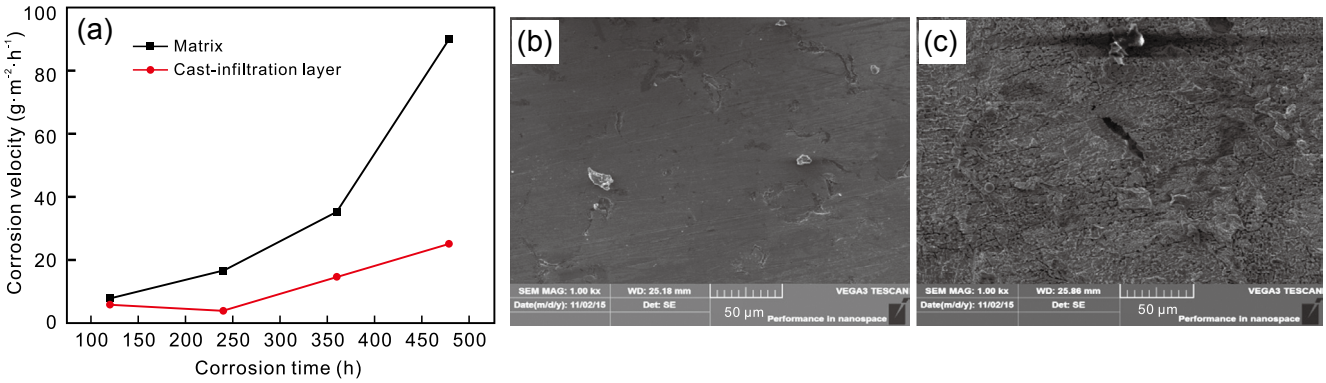

Fig. 7: Variation of corrosion rates of casting-infiltration layer with 35wt.% Ti and ZG45 steel matrix with dipping time in 10wt.% NaCl solution (a), surface morphology (b) and ZG45 steel matrix of casting-infiltration layer (c) after dipping in 10wt.% NaCl solution for 480 h

on the surface of the casting-infiltration layer [Fig. 7(c)]. It can be concluded that the casting-infiltration layer forms a good metallurgical bonding with ZG45 steel matrix, and provides an adequate protection for ZG45 steel against corrosion.

4 Conclusions

Ti-Ni alloy powders were prepared by vacuum melting and atomization technology, and then were coated on the cavity wall of a sand mold, where the molten steel was poured. During casting and solidification processes, a lot of heat was released to melt the alloy powders, and accelerated the diffusion and reactions between the alloy powders and the steel matrix, forming a casting-infiltration layer, namely a protective coating.

(1) When the alloy powder containing 35wt.% Ti and the pouring temperature of the steel is 1,650 °C, an optimum casting-infiltration layer with a thickness of ~7 mm is obtained, which forms a good metallurgical bonding with the steel matrix.

(2) The casting-infiltration layer was mainly composed of stable Fe_2Ti, γ-(Fe, Ni) solid solution and a small amount of metallic Ti gathered around Fe_2Ti phase.

(3) In 3.5wt.% NaCl and 1 mol·L^{-1} H_2SO_4 solutions, the cast-infiltration layer has a higher self-corrosion potential, and thus possesses an enhanced corrosion resistance compared with the matrix, which is also ascertained by a larger capacitance-reactance arc radius of the casting-infiltration layer.

(4) In static corrosion tests in 10wt.% NaCl, a passivation film is formed on the surface of the casting-infiltration layer, which hinders or slows down the corrosion reactions, so there are no obvious traces of corrosion on the surface of casting-infiltration layer after dipping for 480 h. However, many corrosion holes and a small number of transverse grooves appear on the ZG45 steel matrix.

Acknowledgement

This study was financially supported by the National Key R&D Program of China (Grant No. 2016YFB0300603).

References

[1] Baddoo N R. Stainless steel in construction: A review of research, applications, challenges and opportunities. Journal of Constructional Steel Research, 2008, 64(11): 1199–1206.
[2] Yi D W, Shi Y P, Fu H G, et al. Microstructures and erosion-corrosion behavior of Fe-B alloy containing chromium and nickel. China Foundry, 2019, 16: 307–312.
[3] Zhu Z H, Zhang W D, Tu X H, et al. Effect of sigma phase precipitation on microstructure and properties of cast ZG0Cr26Ni5Mo3Cu3 duplex stainless steel under different heat treatments. China Foundry, 2018, 15: 182–188.
[4] Han W J, Li Y Z. The market opportunity and technical evaluation for the spherical steel structure application in China. Journal of Constructional Steel Research, 1998, 46(1–3): 400.
[5] Miao C Q, Li R, Yu J. Effects of characteristic parameters of corrosion pits on the fatigue life of the steel wires. Journal of Constructional Steel Research, 2019: 105879.
[6] Miao C Q, Li R, Yu J. Corrosion protection and assessment of weathering steel highway structures. Journal of Constructional Steel Research, 2010, 66(10): 1174–1185.
[7] Liu H X, Huang F, Yuan W, et al. Essential role of element Si in corrosion resistance of a bridge steel in chloride atmosphere. Corrosion Science, 2020, 173(15): 108758.
[8] Shi J J, Ming J, Wang D Q, et al. Improved corrosion resistance of a new 6% Cr steel in simulated concrete pore solution contaminated by chlorides. Corrosion Science, 2020, 174: 108851.
[9] Takashi D, Takeharu A, Takeo K, et al. In situ investigation of CO_2 corrosion in Cr-containing steels in CO_2-saturated salt solution at elevated temperatures and pressures. Corrosion Science, 2020: 108931.
[10] Pan K M, Yang Y P, Wei S Z, et al. Oxidation behavior of Mo-Si-B alloys at medium-to-high temperatures. Journal of Materials Science and Technology, 2021, 60: 113–127.
[11] Metiko-Hukovi M, Babi R, Gruba Z, et al. High corrosion resistance of austenitic stainless steel alloyed with nitrogen in an acid solution. Corrosion Science, 2011, 53: 2176–2183.
[12] Elivelton A F, Raone C De C Silva, Larissa A T C, et al. Is duplex stainless steel more corrosion resistant than 316L in aqueous acid chloride-containing environments at temperatures higher than 100 °C. Corrosion Engineering Science and Technology, 2018, 53(7): 502–509.
[13] Pardo A, Merino M C, Coy A E, et al. Effect of Mo and Mn additions on the corrosion behaviour of AISI 304 and 316 stainless steels in H_2SO_4. Corrosion Science, 2008, 50(3): 780–794.

[14] Ilevbare G O, Burstein G T. The role of alloyed molybdenum in the inhibition of pitting corrosion in stainless steels. Corrosion Science, 2001, 43(3): 485–513.
[15] Ivan D R, Evelien V B, Karen L, et al. Study of tin corrosion: the influence of alloying elements. Journal of Cultural Heritage, 2004, 5(2): 189–195.
[16] Nam N D, Kim M J, Jang Y W, et al. Effect of tin on the corrosion behavior of low-alloy steel in an acid chloride solution. Corrosion Science, 2010, 52(1): 14–20.
[17] Pardo A, Merino M C, Carboneras M, et al. Pitting corrosion behaviour of austenitic stainless steels with Cu and Sn additions. Corrosion Science, 2007, 49(2): 510–525.
[18] Pardo A, Merino M C, Carboneras M, et al. Influence of Cu and Sn content in the corrosion of AISI 304 and 316 stainless steels in H_2SO_4. Corrosion Science, 2006, 48(5): 1075–1092.
[19] Girot F A, Quenisset J M, Naslain R. Discontinuously reinforced aluminum matrix composites. Composites Science and Technology, 1987, 30(3): 155–184.
[20] Walker J A. Processing and properties of discontinuously reinforced aluminum composites. JOM, 1991, 43(8): 8–15.
[21] Li Q, Lei T C, Chen W Z. Microstructural characterization of WCp reinforced Ni-Cr-B-Si-C composite coatings. Surface and Coatings Technology, 1999, 114(2–3): 285–291.
[22] Zhang G L, Wang J L, Liu Y F, et al. Properties of TiN coating on 45# steel for inner surface modification by grid-enhanced plasma source ion implantation method. Chinese Physics, 2004, 13(8): 1309–1314.
[23] Uusitalo M A, Vuoristo P M J, AMäntylä T. High temperature corrosion of coatings and boiler steels below chlorine-containing salt deposits. Corrosion Science, 2004, 46(6): 1311–1331.
[24] Lee H S, Hong S. H. Pressure infiltration casting process and thermophysical properties of high volume fraction SiCp/Al metal matrix composites. Materials Science and Technology, 2003, 19(8): 1057–1064.
[25] Yang D C. Study on alloyed surface layer of wear resistant castings by evaporable pattern castings infiltration process. Advanced Materials Research, 2012, 538–541: 247–250.
[26] Guo C Q, Shi A J, Han J W. Microstructures of surface alloyed high manganese cast steels. International Conference on Material Science and Application, 2019: 84–88.
[27] Li H X, Yu H, Zhou T, et al. Effect of tin on the corrosion behavior of sea-water corrosion-resisting steel. Materials & Design, 2015, 84: 1–9.
[28] Szymański Ł, Olejnik E, Tokarski T, et al. Reactive casting coatings for obtaining in situ composite layers based on Fe alloys. Surface and Coatings Technology, 2018, 350(25): 346–358.
[29] Zhao N N, Xu Y H, Wang J F, et al. Microstructure and kinetics study on tantalum carbide coating produced on gray cast iron in situ. Surface and Coatings Technology, 2016, 286(25): 347–353.
[30] Yang G R, Hao Y, Song W M, et al. Effects of some parameters on formation and structure of infiltrated (surface) layer prepared by vacuum infiltration casting technique. Surface and Coatings Technology, 2006, 201(3–4): 1711–1717.
[31] Kandavel T K, Chandramouli R, Karthikeyan P. Influence of alloying elements and density on aqueous corrosion behaviour of some sintered low alloy steels. Materials & Design, 2012, 40: 336–342.
[32] Hashimoto K, Asami K, Kawashima A, et al. The role of corrosion-resistant alloying elements in passivity. Corrosion Science, 2007, 49: 42–52.
[33] Geng H F, Liu F S. Microstructures of Ti-Ni-Fe wire after severe cold-drawing and annealing. Rare Metals, 2013, 32: 550–554.
[34] Zhang B, Ye F, Liu Q, et al. Study on dielectric properties of $BADC_y$/Ni0.5Ti0.5NbO4 composites fabricated by freeze casting combined with vacuum assisted infiltration process. Journal of Materials Science, 2016, 27(11): 11986–11994.
[35] Gupta K P. The Fe-Ni-Ti system update (Iron-Nickel-Titanium). Journal of Phase Equilibria, 2001, 22(2): 171–175.
[36] Du P, Li J Z, Zhao Y L, et al. Corrosion characteristics of Al alloy/galvanized-steel Couple in NaCl solution. International Journal Electrochemical Science, 2018, 13: 11164–11179.